Longitudinal and transverse spin dynamics of donor-bound electrons in fluorine-doped ZnSe: Spin inertia versus Hanle effect

F. Heisterkamp,[1] E. A. Zhukov,[1] A. Greilich,[1] D. R. Yakovlev,[1,2] V. L. Korenev,[1,2] A. Pawlis,[3,4] and M. Bayer[1,2]

[1]*Experimentelle Physik 2, Technische Universität Dortmund, 44221 Dortmund, Germany*

[2]*Ioffe Physical-Technical Institute, Russian Academy of Sciences, 194021 St. Petersburg, Russia*

[3]*Peter Grünberg Institute, Forschungszentrum Jülich, 52425 Jülich, Germany*

[4]*Department Physik, Universität Paderborn, 33098 Paderborn, Germany*

The spin dynamics of strongly localized donor-bound electrons in fluorine-doped ZnSe epilayers is studied using pump-probe Kerr rotation techniques. A method exploiting the spin inertia is developed and used to measure the longitudinal spin relaxation time T_1 in a wide range of magnetic fields, temperatures, and pump densities. The T_1 time of the donor-bound electron spin of about 1.6 μs remains nearly constant for external magnetic fields varied from zero up to 2.5 T (Faraday geometry) and in a temperature range 1.8–45 K. These findings impose severe restrictions on possible spin relaxation mechanisms. In our opinion they allow us to rule out scattering between free and donor-bound electrons, jumping of electrons between different donor centers, scattering between phonons and donor-bound electrons, and with less certainty charge fluctuations in the environment of the donors caused by the 1.5 ps pulsed laser excitation.

I. INTRODUCTION

Fluorine-doped ZnSe recently emerged as a promising material system in the field of solid-state quantum information technologies. So far indistinguishable single-photon sources and optically controllable electron spin qubits were demonstrated in this material [1–3]. Long electron spin coherence times and spin relaxation times are one of the prerequisites for a system to be suited for quantum information technologies [4]. To obtain access to these times, optical techniques have proved to be an adequate measurement tool.

Generally, the phenomenon of optical orientation is used to create the initial spin orientation [5]. It involves two processes: the photogeneration of spin-oriented carriers by absorption of circularly polarized light and the possible spin relaxation with the characteristic time τ_S during the lifetime τ of these carriers [5]. In order to determine absolute values of these times one often uses an "internal clock" of the system: The periodic Larmor precession of the electron spins about an external magnetic field with the frequency $\Omega_L = \mu_B g_e B/\hbar$ can be used as such a clock. Here μ_B is the Bohr magneton and g_e is the Landé factor of the electrons. One of the common methods to study spin lifetimes $T_S = 1/(1/\tau + 1/\tau_S)$ in atoms [6,7] and in solid-state systems [5,8] is the measurement of the Hanle effect. The Hanle effect analyzes the decrease of the carrier spin polarization (typically via the circular polarization degree of photoluminescence) in a transverse magnetic field so that it also employs the clock defined by the Larmor precession. For relatively strong magnetic fields, for which the spin lifetime T_S is long compared to the time scale determined by the Larmor precession frequency Ω_L ($T_S \gg 1/\Omega_L$), the electron spins perform many revolutions during their lifetime [5]. Thus, the spin polarization along the direction of observation decreases with increasing transverse magnetic field. The Hanle curve describes this behavior. Its half-width at half maximum is given by $B_{1/2} = \hbar/(\mu_B g_e T_S)$, so the spin lifetime T_S can be obtained by measuring the Hanle curve, if the g factor is known [9–11].

The method based on the Hanle effect employs the relaxation time approximation, in which the spin dynamics is described by one or a few exponents. It is a fair approximation, if the relaxation is caused, for example, by processes with short correlation times (Markovian processes) since these short correlation times lead to dynamic averaging over magnetic fields of different origin, acting on the electron. However, this approximation is violated for strongly localized electrons, when the correlation time of the electron with the donor exceeds the precession period of the electron spin in the hyperfine field of the nuclei. The width of the Hanle curve for donor-bound electron spins is determined by the relatively rapid precession in static nuclear fields [12,13], i.e., by the spin dephasing time T_2^*, and not by the longitudinal spin relaxation time T_1 or τ_S, which are both equal to T_S in the limit of zero excitation density. T_1 or τ_S can be much longer than the precession period in the frozen nuclear field. Dephasing in static fields is reversible and to eliminate their effect the spin-echo method can be used [14]. However, this leads to a complication of experiments on the irreversible spin dynamics, designed to determine the T_1 time. While the inhomogeneous spin dephasing time T_2^* can be seen as a lower limit of the spin coherence time T_2, which is the important quantity for quantum information technologies, the T_1 time is used to estimate the upper limit of T_2 ($T_2 \leqslant 2T_1$) [15].

We propose a different approach to measure the spin lifetime, which does not rely on the precession of the spins in a magnetic field applied in the Voigt geometry. This method uses an external clock instead of an internal one, namely the periodic polarization modulation of the exciting light with the modulation frequency f_m, and exploits the inertia of the spins: when switching the helicity of the light the steady-state value of the electron spin polarization is reached within the characteristic time T_S. At low modulation frequencies $2\pi f_m \ll 1/T_S$ the electron spin polarization can overcome the spin inertia and reach its steady-state value for a particular laser polarization period. For high modulation frequencies $2\pi f_m \geqslant 1/T_S$, on the other hand, the electron

spin polarization remains reduced since it cannot reach its steady-state value within a duty cycle with fixed circular polarization. The fall or rise of the spin polarization in dependence on the modulation frequency corresponds to the spin lifetime. With this method one can measure the spin lifetime in a weak magnetic field, when the dynamics of the average spin is determined by relaxation processes in random fields that are not subject to dynamic averaging, i.e., when the method based on the Hanle effect cannot provide the time T_S.

A similar method was used by Akimov *et al.* [16,17] to study the electron spin dynamics in epitaxial CdSe/ZnSe quantum dots. The method combines time- and polarization-resolved measurements of the emission from the trion singlet ground state with helicity modulation of the exciting light. However, the spin polarization was not measured in dependence of the modulation frequency by Akimov *et al.*, so our method can be seen as an advancement. Fras *et al.* performed differential transmission measurements of InAs/GaAs quantum dots using the optical pump-probe technique [18]. Here, in addition to time-resolved measurements a technique called dark-bright time scanning spectroscopy was used, where the intensity of the exciting beam was modulated to measure in the frequency domain. In contrast to this Colton *et al.* measured the spin lifetime T_1 in a modulation-doped (100) GaAs/AlGaAs quantum well directly in the time domain by employing a pump-probe technique with an electronically controlled time delay between pump and probe [15]. This scheme allowed very long delays up to the μs range.

In this paper we investigate the spin dynamics of the strongly localized, donor-bound electrons in fluorine-doped ZnSe epilayers in a wide range of magnetic fields, temperatures, and pump densities using the spin inertia method. The paper is organized as follows. Section II provides details of the experimental techniques and the studied sample. Section III describes the experimental results. Section IV is devoted to the theoretical consideration of the spin inertia effect and the modeling of the experimental data. The discussion of the spin relaxation mechanisms is done in Sec. V. There we also assess the applicability of the spin inertia method to various spin systems.

II. EXPERIMENTAL DETAILS

The studied sample consists of three layers grown by molecular-beam epitaxy on (001)-oriented GaAs substrate. A thin ZnSe buffer layer reduces the strain induced by the II-VI on III-V heteroepitaxy. The ZnSe layer is followed by a 20-nm-thick $Zn_{1-x}Mg_xSe$, $x < 0.15$ barrier layer, which prevents carrier diffusion into the substrate. The fluorine-doped, 70-nm-thick ZnSe epilayer is grown on top of this barrier layer. It has a fluorine concentration of about 1×10^{15} cm^{-3}. For the optical properties of this sample and for information on the electron spin dephasing we refer to Ref. [19].

The sample is placed in a vector magnet system consisting of three superconducting split coils oriented orthogonally to each other [20]. It allows us to switch the magnetic field from the Faraday geometry (magnetic field $\mathbf{B}_F$ parallel to the sample growth axis and the light wave vector) to the Voigt geometry (magnetic field $\mathbf{B}_V$ perpendicular to the sample growth axis
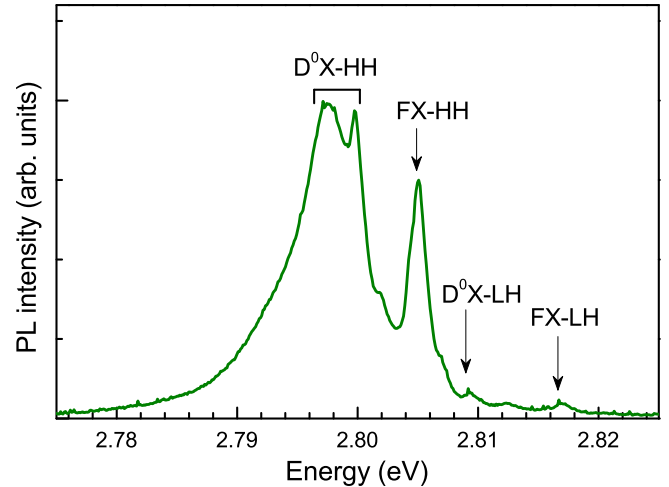

FIG. 1. (Color online) PL spectra of the fluorine-doped ZnSe epilayer measured at $B = 0$ T for $T = 1.8$ K.

and the light wave vector). The switching can be performed by using the respective pairs of split coils and does not require any changes of the optical alignment. Therefore we can measure in different magnetic field geometries with exactly the same adjustment and overlap of the pump and probe beams on the sample. The measurements are performed at low temperatures with the sample either immersed in pumped liquid helium at $T = 1.8$ K or cooled with a controlled helium gas flow (up to 45 K). Photoluminescence (PL) spectra for sample characterization are excited using a continuous-wave (cw) laser with a photon energy of 3.05 eV and detected with a Si-based charge-coupled device (CCD) camera attached to a 0.5-m spectrometer.

We use the pump-probe technique to study the electron spin dynamics by time-resolved Kerr rotation (TRKR). The electron spin coherence is created by circularly polarized pump pulses of 1.5 ps duration (spectral width of about 1 meV) emitted by a mode-locked Ti:sapphire laser operating at a repetition frequency of 75.7 MHz (repetition period $T_R = 13.2$ ns). The induced electron spin coherence is measured by linearly polarized probe pulses of the same photon energy as the pump pulses (degenerate pump-probe scheme). A mechanical delay line is used to scan the time delay between the probe and pump pulses. The photon energy is tuned into resonance with the donor-bound heavy-hole exciton (D^{0}X-HH) at about 2.80 eV (see Fig. 1). To obtain this photon energy a beta-barium borate (BBO) crystal is used to double the frequency of the light generated by the Ti:sapphire laser. The pump helicity is modulated between σ^+ and σ^- polarization by an electro-optical modulator (EOM), so that on average the sample is equally exposed to left- and right-circularly polarized pump pulses. The modulation frequency is varied between 10 kHz and 700 kHz. The photogenerated spin polarization results in a rotation of the polarization plane of the reflected, initially linearly polarized probe pulses due to the magneto-optical Kerr effect. The Kerr rotation (KR) angle of the probe beam is measured by a 10 MHz balanced photoreceiver with adjustable gain and bandwidth, connected to a lock-in amplifier. The pump density

is varied in the range $P_{pump} = 0.2$–4.2 W/cm², which is low enough to ensure a linear response of the KR amplitude to the pump density and well below a π pulse. The probe density (P_{probe}) is about one order of magnitude smaller than the pump density.

We use three different implementations of the pump-probe Kerr rotation method:

(1) The time-resolved Kerr rotation configuration, where the Kerr rotation angle is measured in dependence on the time delay between the pump and probe pulses with the magnetic field applied in the Voigt geometry. In this case the Larmor precession of the electron spin polarization around the magnetic field axis results in a signal which is a periodic function of the time delay and whose amplitude decreases with increasing time delay. Using this configuration one can determine the g factor of the carriers and the inhomogeneous spin dephasing times T_2^* in the limit $T_2^* < T_R$ [19].

(2) The resonant spin amplification (RSA) configuration [4,21,22] is used to determine T_2^* when this time is comparable to or greater than the laser repetition period T_R. Here the time delay between pump and probe is fixed at a small negative value ($\Delta t \approx -20$ ps) and one measures the KR angle in dependence on the magnetic field applied in the Voigt geometry in the range from -20 to $+20$ mT. At certain magnetic fields the electrons spins precess in phase with the laser repetition frequency and one observes an increased Kerr rotation signal.

(3) In the polarization recovery (PR) configuration the electron spin polarization is also detected at a fixed, small negative time delay. The KR signal is measured in dependence of the magnetic field applied in the Faraday geometry. The electron spin polarization, which is photogenerated along the magnetic field direction, does not exhibit Larmor precession then. Still it is decreased by the nuclear hyperfine fields, if the external magnetic field is small compared to these fields. The effect of the hyperfine fields is suppressed with increasing external magnetic field. By varying the pump helicity modulation frequency one can measure the longitudinal spin relaxation time T_1 of the electrons. We will mostly use this implementation to study the spin dynamics of the donor-bound electrons.

Note that the measurement of the KR signal at negative time delay, prior to the pump pulse, used in the RSA and PR configurations, greatly simplifies the interpretation of the signal origin. These signals can only arise from long-living spins, whose lifetime exceeds $T_R = 13.2$ ns. This is typically much longer than the exciton recombination time, so that the measured signals can originate only from resident electrons, which are bound to donors at low temperatures.

In addition, we also perform pump-probe experiments using a cw pump and a pulsed probe. For these measurements a cw Ti:sapphire laser with intracavity second harmonic generation is used as the pump, and the probe pulses are generated from the laser system described above. This configuration allows us to set the pump and the probe laser at different photon energies, i.e., to perform two-color nondegenerate pump-probe measurements. Thereby we measure the PR and the suppression of the KR signal in the Voigt geometry (the Hanle curve), to investigate possible influences of pulsed excitation on the spin relaxation.

III. EXPERIMENTAL RESULTS

Figure 1 shows the PL spectrum of the studied sample, measured at zero magnetic field for a temperature of $T = 1.8$ K. The spectrum exhibits the following emission lines: Donor-bound heavy-hole exciton (D^0X-HH) at 2.7970–2.7997 eV, free heavy-hole exciton (FX-HH) at 2.8045 eV, donor-bound light-hole exciton (D^0X-LH) at 2.8092 eV, and free light-hole exciton (FX-LH) at 2.8167 eV. The strain induced by the II-VI on III-V heteroepitaxy lifts the light-hole and heavy-hole degeneracy [19].

Results of pump-probe measurements in all three experimental configurations are illustrated in Fig. 2. Results obtained with the TRKR and RSA configurations were considered in detail in Ref. [19] and are given here for comparison with the PR data. Furthermore, they provide important supplementary information on the donor-bound electron spins.

Figures 2(a) and 2(b) show time-resolved Kerr rotation signals measured at a temperature of $T = 1.8$ K for resonant D^0X-HH excitation. While the spectrum in Fig. 2(a) is measured at zero external magnetic field, in Fig. 2(b) a magnetic field of $B_V = 0.42$ T is applied in the Voigt geometry and the observed oscillations reflect the Larmor precession of the electron spin polarization. Note that these oscillations are long living and do not fully decay during the time interval $T_R = 13.2$ ns between subsequent pump pulses, as can be seen from the considerable signal amplitude at negative time delays. As has been reported in Ref. [19] the exciton lifetime in ZnSe is shorter than 250 ps and the long-living TRKR signal originates from the coherent spin precession of the localized donor-bound
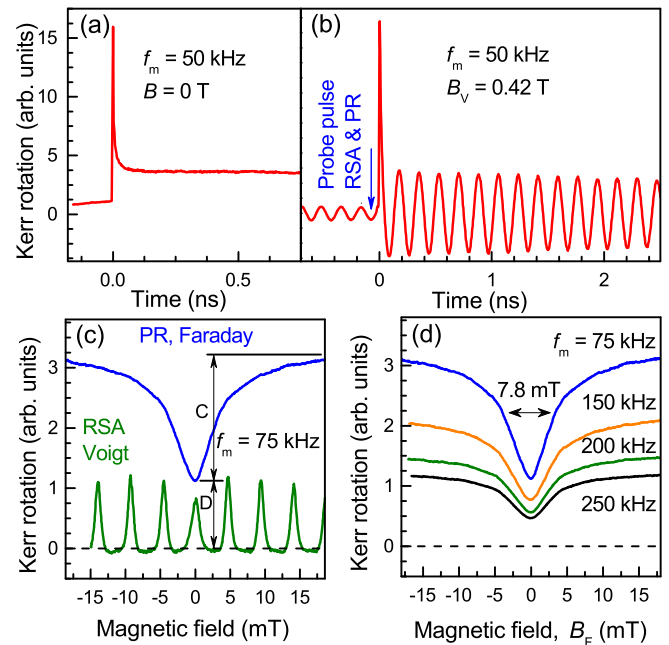

FIG. 2. (Color online) TRKR results measured for resonant D^0X-HH excitation (2.7986 eV) at $T = 1.8$ K. (a) and (b) KR signals in dependence on the time delay at $f_m = 50$ kHz and $P_{pump} = 1.6$ W/cm². The arrow marks the time delay at which the RSA and PR signals are detected. (c) PR and RSA signals measured at $f_m = 75$ kHz. (d) PR signals measured at different modulation frequencies. In panels (c) and (d) $P_{pump} = 0.5$ W/cm².

electrons. The relatively large binding energy to these donors of 29 meV [23] provides strong electron localization and makes the spin coherence robust even at elevated temperatures up to 40 K [19]. A g factor of the donor-bound electron of $|g_e| = 1.13 \pm 0.02$ is evaluated from the period of the signal oscillations in Fig. 2(b), see Ref. [19].

Due to the long decay of the TRKR signal amplitude it is difficult to evaluate the electron spin dephasing time T_2^* by fitting the amplitude decay in these measurements. Instead the RSA technique was used for that purpose; for details see Ref. [19]. An example of a RSA signal is shown by the green line in Fig. 2(c). It consists of periodic peaks with a width of about 1 mT.

To extract the spin dephasing time around zero field from these data the following equation is fitted to the measured signal, using T_2^* as the only free fitting parameter [19,21]:

$$\Theta_{KR}(B) \propto e^{-\frac{\Delta t + T_R}{T_2^*}} \frac{\cos(\Omega_L \Delta t) - e^{\frac{T_R}{T_2^*}} \cos[\Omega_L (\Delta t + T_R)]}{\cos(\Omega_L T_R) - \cosh(T_R/T_2^*)}.$$
(1)

Note that here we consider $T_S \equiv T_2^*$. The time evaluated from the best fit is $T_2^* = 33$ ns.

The polarization recovery signal measured for the same experimental conditions as the RSA signal (only the magnetic field geometry is changed from Voigt to Faraday) is shown in Fig. 2(c) by the blue line. The PR curve has a minimum at zero magnetic field, increases with increasing B_F, and saturates at fields exceeding 20 mT. Obviously, the polarization recovery is caused by suppression of the depolarization of the electron spin along the magnetic field direction. We tentatively relate the depolarization around zero field to the effect of the fluctuating nuclear hyperfine fields; more details will be given in the discussion below.

As shown in Fig. 2(c), the amplitude of the zero RSA peak is a little smaller than the amplitude of the neighboring peaks. This may be due to the following factors: (1) A small, additional magnetic field component perpendicular to B_V can lead to a reduction of the amplitude of the RSA peak at zero field [20]. This component can occur if there is a small inclination (about $1°–2°$) of the sample plane with respect to the **k** vector (either horizontally or vertically). (2) An additional nuclear field induced at B_V may also lead to a reduction or an increase of the amplitude of the zero RSA peak [24].

Figure 2(d) shows PR signals, measured for different pump helicity modulation frequencies, f_m, varied from 75 up to 250 kHz. The magnitude of the PR signal decreases for higher f_m, while the full width at half maximum (FWHM) of the dip around the zero magnetic field of about 7.8 mT and the overall shape of the PR curves remain the same. These findings suggest that the inverse electron spin relaxation time falls in the examined frequency range.

To study this in more detail the PR amplitude in dependence on the modulation frequency is measured at $B_F = 5$ mT for two pump densities. The PR amplitude for both pump densities, shown by the symbols in Fig. 3(a), remains constant for low modulation frequencies on the order of a few 10 kHz, while it rapidly decreases above 100 kHz. Model calculations shown by the red lines [according to Eq. (11) in Sec. IV] allow us to
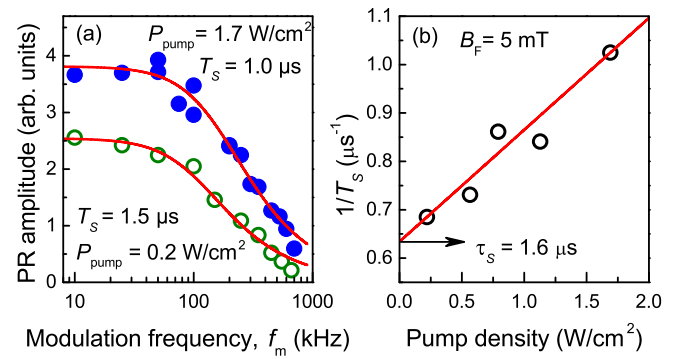

FIG. 3. (Color online) Spin dynamics measured with the PR technique at $B_F = 5$ mT for $T = 1.8$ K. (a) PR amplitude in dependence on f_m for two pump densities of 0.2 and 1.7 W/cm². Red lines show the fits to the data based on our theoretical model [see Eq. (11) in Sec. IV], which is used to determine the spin lifetime T_S. (b) Inverse spin lifetime $1/T_S$ in dependence on the pump density. Red line represents a linear fit [see Eq. (2)] to the data, which is used to extrapolate the spin relaxation time $\tau_S = 1.6$ μs.

evaluate the spin lifetime $T_S = 1.5$ μs for $P_{pump} = 0.2$ W/cm² and $T_S = 1.0$ μs for $P_{pump} = 1.7$ W/cm². Note that the spin lifetimes T_S are on the order of the "cutoff frequency" of 100 kHz ($1/T_S \approx 100$ kHz) of the PR amplitude in dependence on f_m. The spin lifetime in dependence on the pump density is plotted in Fig. 3(b). The decrease of the PR amplitude with increasing f_m is the key result of this study. In the following we present details of its change with varying magnetic field strength and temperature in order to obtain comprehensive information on the spin dynamics of the donor-bound electrons in ZnSe.

The blue circles in Fig. 4(a) illustrate the spin relaxation time τ_S, determined with our model, in dependence on the magnetic field, varied from zero to 20 mT. The black line shows the corresponding PR signal at $f_m = 75$ kHz. The spin relaxation time remains constant within the accuracy of our method in this B_F range. The PR signal in an extended magnetic field range up to 0.5 T is shown in Fig. 4(b). The signal remains nearly constant in the magnetic field range from 0.02 to 0.5 T. In this range its amplitude decreases by a factor of 15, when f_m is changed from 75 kHz to 400 kHz (note the multiplication factor of 5 in the figure). For higher fields we perform measurements each 0.5 T in the range 1.0–2.5 T. For each field four modulation frequencies are examined [see Fig. 4(c)]. For all measured f_m the PR amplitude is independent of the magnetic field strength. Its frequency dependence is fitted according to Eq. (11) using the same fitting parameter $T_S = 1.1$ μs for all measured magnetic fields. An important experimental result of Fig. 4 is that the PR amplitude in dependence on B_F considerably increases from zero to 20 mT, but then remains constant in the range from 20 mT up to 2.5 T.

The shape of the PR amplitude as function of the modulation frequency is maintained in the temperature range from 1.8 up to 45 K, as illustrated by the experimental data presented in Fig. 5, where results for $T = 1.8$, 30, and 45 K are compared. The PR amplitude decreases slightly by less than 40% for elevated temperatures and has been normalized to $T = 1.8$ K
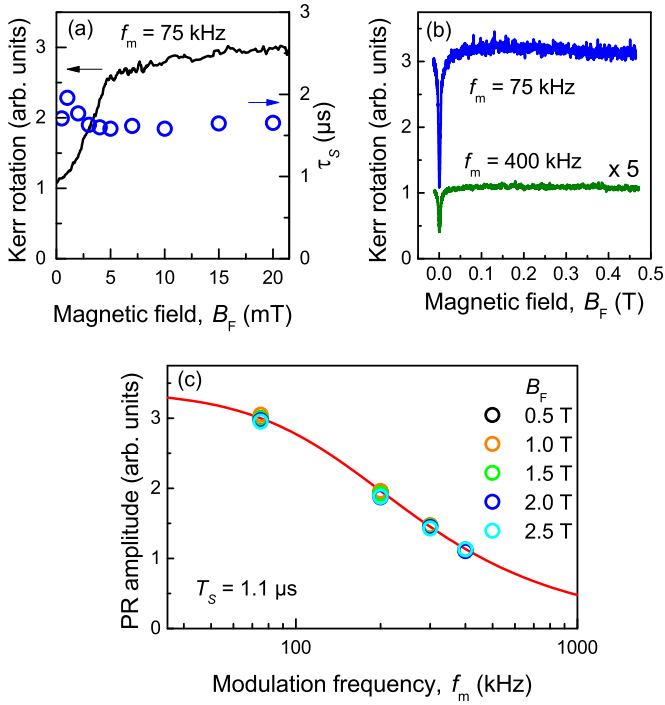
FIG. 4. (Color online) Experimental results measured at $T =$ 1.8 K. (a) Blue circles give the spin relaxation time τ_S in dependence on the magnetic field. Black line shows a typical PR signal. $P_{pump} =$ 1.7 W/cm². (b) PR signals in dependence on B_F for $f_m = 75$ kHz (blue line) and 400 kHz (green line, multiplied by factor of 5). $P_{pump} = 2.4$ W/cm². (c) Modulation frequency dependence of the PR amplitude measured in different magnetic fields B_F. $P_{pump} =$ 2.4 W/cm². Red line shows fit to the data according to Eq. (11) with the fit parameter $T_S = 1.1$ μs.

at 100 kHz. The shape of the frequency dependence remains almost the same evidencing that the spin dynamics of the donor-bound electrons does not change at $T < 45$ K.
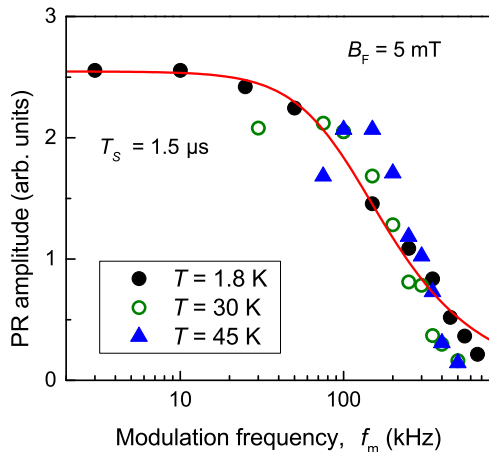

FIG. 5. (Color online) PR amplitude in dependence on the modulation frequency measured at three different temperatures. Data are normalized to each other at $f_m = 100$ kHz. $P_{pump} = 0.4$ W/cm². Red line shows fit to the data at $T = 1.8$ K according to Eq. (11) with the fit parameter $T_S = 1.5$ μs.

The spin relaxation mechanism of optically oriented carriers may depend on whether cw or pulsed photoexcitation is used. Excitation of spin systems with short pulses of picosecond duration may induce perturbations assisting the spin relaxation. We have measured the T_1 time using a cw pump and obtained the same results. We compared the shape (width) of the PR curves and found it to be exactly the same. Furthermore, we have measured the Hanle curve using a cw pump. Its width is very close to the width of the RSA curve which is a similar result to that in Ref. [25], where the influence of a pulsed excitation was investigated for CdTe/(Cd,Mg)Te quantum wells.

IV. THEORY

In this section we develop a theoretical approach to describe the PR effect and its dependence on the pump helicity modulation frequency and the pump density. It will be used to model the experimental data and to determine the characteristic times for the electron spin dynamics.

In n-type semiconductors the process of optical orientation results from the replacement of unpolarized resident electrons with photogenerated, spin-oriented electrons [5]. The electrons lose their spin orientation due to spin relaxation with time τ_S. Also their recombination with photogenerated holes will reduce the macroscopic electron spin polarization. As a result, the lifetime of the photogenerated electrons, $\tau = n_0/G$, depends on the rate of electron-hole generation G, and on the resident electron concentration n_0. The spin lifetime T_S,

$$1/T_S = 1/\tau + 1/\tau_S, \qquad (2)$$

determines the time until the steady-state spin polarization is reached by optical pumping.

Although we use a pulsed laser, it will be treated as a cw laser, since even at relatively high modulation frequencies, e.g., $f_m = 200$ kHz, the following relation holds:

$$\frac{1}{f_m} = 5 \text{ μs} \gg T_R = 13.2 \text{ ns}. \qquad (3)$$

Thus, the sample is exposed to almost 200 pump pulses of each helicity during one modulation cycle, which can be approximated by a cw excitation with the same average power density.

In our experiment in the polarization recovery configuration the pump helicity is modulated, so that the spin polarization is switched between steady-state polarizations with opposite signs. On the one hand, if the modulation frequency is so small that the period with constant pump helicity is much longer than the spin lifetime ($2\pi f_m \ll 1/T_S$), the average spin polarization seems to follow the pump polarization with negligible inertia (see Fig. 6). On the other hand, if the pump helicity modulation is so fast that the period with constant pump helicity is comparable to or shorter than the spin lifetime ($2\pi f_m \gtrsim 1/T_S$), the spin polarization cannot reach its steady-state value and the Kerr rotation signal is decreased significantly.

We consider the case when the electron spin polarization **S** is generated along the z axis, i.e., when the light wave vector of the pump laser is parallel to the z axis (**k** ∥ **z**). First, we analyze the situation in the absence of static magnetic fields. The following kinetic equation describes the dynamics of the
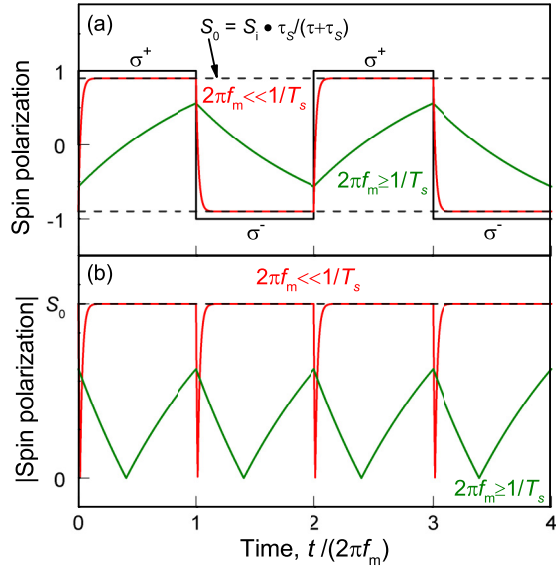
FIG. 6. (Color online) Illustration of the effect of electron spin inertia for pump helicity modulation with frequency f_m. The red and green lines show the limits of $2\pi f_m \ll 1/T_S$ and $2\pi f_m \gtrsim 1/T_S$, respectively. (a) Illustration of the spin polarization S_z along the direction of observation for two modulation periods: While in the first case the spin polarization follows the laser polarization without inertia and always reaches the steady-state value S_0 in a fixed laser polarization period, the spin polarization cannot reach S_0 during such a period, when the modulation is fast compared to the time scale given by the spin lifetime T_S. (b) Modulus of the spin polarization $|S_z(t)|$ for both limits. While in the first case ($2\pi f_m \ll 1/T_S$, red line) $|S_z|$ is equal to $|S_0|$ almost during the whole modulation period except for a small decrease, when the sign of the polarization is switched, the modulus of the spin polarization is strongly decreased during the whole modulation period for $2\pi f_m \gtrsim 1/T_S$.

electron spin polarization [5]:

$$\frac{dS_z(t)}{dt} = \frac{S_i - S_z(t)}{\tau} - \frac{S_z(t)}{\tau_S}. \tag{4}$$

The initially generated spin polarization $\mathbf{S_i} = (0,0,S_i)$ depends on the laser polarization and optical selection rules. The first term on the right side describes the polarization injection (S_i/τ) and escape due to electron recombination ($-S_z/\tau$) with time τ, and the second term describes the spin relaxation with time τ_S.

The stationary solution for a constant circular polarization of the pump is given by

$$S_z = S_0 = S_i \frac{\tau_S}{\tau_S + \tau} = S_i \frac{G\tau_S}{G\tau_S + n_0}. \tag{5}$$

For pump helicity modulation with the frequency f_m we have to solve the nonstationary Eq. (4). Combining Eqs. (2) and (4), we find

$$\frac{dS_z(t)}{dt} = \frac{S_0(t) - S_z(t)}{T_S}. \tag{6}$$

In our experiment $S_0(t) = S_i(t)\frac{\tau_S}{\tau + \tau_S}$ is an alternating signal of rectangular pulses with a constant amplitude $|S_0|$, a duty cycle of 0.5, and the modulation frequency f_m.

In the experiment we measure a signal, which is proportional to $n_0 S_z$. The spin polarization along the direction of observation $S_z(t)$ is oscillating with the modulation frequency f_m. This means that we measure the following correlator:

$$L(f_m) = \langle S_z(t) \exp(i2\pi t/T_m)\rangle|_{T_m}$$

$$= \int_0^{T_m} \frac{S_z(t)\exp(i2\pi t/T_m)}{T_m} dt. \tag{7}$$

The averaging is done over the pump modulation period $T_m = 1/(2\pi f_m)$. As a result, the task consists of two steps: (i) determine $S_z(t)$ and (ii) calculate the correlator according to Eq. (7). The calculations show that the spin polarization along the direction of observation, $S_z(t)$, is a periodic function with the period T_m of the pump helicity modulation

$$S_z(t) = |S_0| \left(1 - \frac{2e^{-\frac{t}{T_S}}}{1 + e^{-\frac{T_m}{2T_S}}}\right), \tag{8}$$

in the half cycles in which $S_0(t) = +|S_0|$,

$$S_z(t) = |S_0| \left\{-1 + 2\left(e^{\frac{T_m}{2T_S}} - \frac{1}{1 + e^{\frac{-T_m}{2T_S}}}\right)e^{-\frac{t}{T_S}}\right\}, \tag{9}$$

in the half cycles in which $S_0(t) = -|S_0|$. Hence it is possible to determine the following correlator (7):

$$L(f_m) = -\frac{2n_0|S_0|}{\pi(i + 2\pi f_m T_S)}. \tag{10}$$

In the experiment the lock-in amplifier records the following signal:

$$|L(f_m)| = \frac{2}{\pi} \frac{n_0|S_0|}{\sqrt{1 + (2\pi f_m T_S)^2}}. \tag{11}$$

Figure 6 schematically illustrates the spin inertia effect and shows how the dependence of the correlator on the modulation frequency and the spin lifetime manifests itself in experiment. Figure 6(a) shows the time-dependent spin polarization along the direction of observation $S_z(t)$ for two modulation periods. In the case of slow modulation compared to the spin lifetime (red line) the spin polarization follows the laser polarization without significant inertia and always reaches the steady-state value $|S_0|$ in a period of fixed laser polarization. However, the spin polarization cannot reach $|S_0|$ during such a period, when the modulation occurs fast compared to the spin lifetime T_S (green line). Note that the time-averaged spin polarization is equal to zero in both cases. However, the lock-in amplifier records the signal, which is proportional to the time-averaged modulus $|S_z|$ of the spin polarization [see Fig. 6(b)]. For $2\pi f_m \ll 1/T_S$ (red line) this time-averaged value is very close to $|S_0|$, while it is clearly smaller than $|S_0|$ in the limit $2\pi f_m \gtrsim 1/T_S$. We denote this inability of the spin polarization to follow the polarization of the exciting light for a fast modulation compared to the spin lifetime as the spin inertia effect.

Investigation of the carrier's spin dynamics by the spin inertia effect can be performed at zero as well as finite external magnetic fields. In a magnetic field the evaluated spin relaxation time τ_S corresponds to the longitudinal spin relaxation time T_1. It is also valid for samples in which the

electron spins are affected by randomly oriented hyperfine fields from the nuclear spin fluctuations [12,13], namely, when the spin dephasing time T_2^* caused by the nuclear fluctuations is considerably shorter than T_1. Note that in this case the method based on the Hanle effect is limited to measurements of the T_2^* time, and not the T_1 time. We discuss this in more detail in Sec. V.

For example, in our fluorine-doped sample the donor-bound electrons are strongly localized. Thus, the dwell time of an electron on a donor is longer than the inhomogeneous dephasing time T_2^* of the ensemble of donor-bound electrons in the frozen hyperfine fields of the nuclei, $\mathbf{B_N}$. The components of the electron spin perpendicular to the hyperfine field decay during T_2^*, while the spin polarization along the hyperfine field direction decays on a much longer time scale $T_1 \gg T_2^*$.

Note that strong static magnetic fields, either the homogeneous external magnetic field $\mathbf{B}$ or the randomly oriented nuclear hyperfine fields $\mathbf{B_N}$ at various donors, would not change the frequency dependence of the signal in Eq. (11). These fields can be accounted for by adding the precession term $\mathbf{\Omega_\Sigma} \times \mathbf{S}$ to Eq. (6):

$$\frac{d\mathbf{S}(t)}{dt} = \frac{\mathbf{S}_0(t) - \mathbf{S}(t)}{T_S} + \mathbf{\Omega_\Sigma} \times \mathbf{S}. \qquad (12)$$

Here $\mathbf{\Omega_\Sigma} = \mu_B g_e \mathbf{B_\Sigma}/\hbar$ is the Larmor frequency of the donor-bound electron in the superposition of both fields $\mathbf{B_\Sigma} = \mathbf{B} + \mathbf{B_N}$. We can consider the nuclear field as static, when the dwell time of the electron on the donor τ_d is long, so that $\tau_d \Omega_N \gg 1$, where $\Omega_N = \mu_B g_e B_N/\hbar$ is the Larmor frequency in the nuclear field.

Equation (12) explicitly accounts for the contribution of the randomly oriented, static hyperfine fields of the nuclei. But it does not mean that other contributions to the electron spin relaxation should be static. For example, spin-orbit, exchange, or other interactions in the considered system can exhibit fast fluctuations and their contribution should be described using the relaxation time approximation. These mechanisms are approximately described by the common spin lifetime T_S. In strong magnetic fields ($T_S \Omega_\Sigma \gg 1$) only the spin component $\mathbf{S}_B$ along the field $\mathbf{B_\Sigma}$ is conserved. By scalar multiplication of Eq. (12) with $\mathbf{\Omega_\Sigma}$ one can show that the z component $\mathbf{S}_B = (\mathbf{SB_\Sigma})\mathbf{B_\Sigma}/B_\Sigma^2$ corresponds exactly to Eq. (6) in which one should replace S_z with $S_{B,z}$ and $S_0(t)$ with $S_{B,0}(t) = S_0(t)B_{\Sigma,z}^2/B_\Sigma^2$. As a result, we obtain the following equation which is similar to Eq. (11) and describes the signal measured with the lock-in amplifier:

$$|L(f_m, B_\Sigma)| = \frac{2}{\pi} \frac{n_0 |S_0|}{\sqrt{1 + (2\pi f_m T_S)^2}} \left\langle \frac{B_{\Sigma,z}^2}{B_\Sigma^2} \right\rangle. \qquad (13)$$

Here the angle brackets mean averaging over a Gaussian distribution of the hyperfine fields [12,13]. Comparing Eqs. (11) and (13) one can see that the signal as a function of the modulation frequency f_m is the same, while in relatively strong magnetic field the time T_S can be a function of the magnetic field, as the spin relaxation is accompanied by the energy transfer equal to the Zeeman splitting of the electron energy. Keep in mind that in the limit of weak excitation densities $T_S(B)$ is equal to $\tau_S(B)$, which in turn is equal to the longitudinal spin relaxation time $T_1(B)$. Therefore, one

can evaluate $T_1(B)$ from the frequency dependence of $L(f_m)$ for any magnetic field.

In the limit of low modulation frequencies ($2\pi f_m T_S \ll 1$) the quasistatic Eq. (13) for the spin polarization is equal to Eq. (27) from Ref. [13] for the polarization in dependence on the magnetic field up to the constant coefficient. Contrary to the frequency dependence, the signal in dependence on the magnetic field $L(B)$ does not have a simple analytical form, but can be discussed qualitatively. At $B = 0$ the averaged random distribution of the nuclear fields decreases the initial polarization degree by a factor of 3 to $S_z = S_0/3$ [26]. A magnetic field in the Voigt geometry decreases the spin polarization S_z due to the Larmor precession of the electron spin (Hanle effect), while a magnetic field in the Faraday geometry stabilizes the spin polarization (PR signal) by suppressing the effect of the nuclear fields, which deviate from the external magnetic field, on the electron spin. The polarization as a function of magnetic field is characterized by the half-width at either half maximum in Voigt geometry $B_{1/2}^V$ or at half minimum in Faraday geometry $B_{1/2}^F$. These fields are controlled by the dispersion of the nuclear field δ_B and it is expected that $B_{1/2}^V = B_{1/2}^F$ [13]. The validity of this approach for the description of the investigated system, the strongly localized, donor-bound electron in fluorine-doped ZnSe, is approved by the "1/3" rule, namely that the polarization at zero field has 1/3 of its maximal value to which it can recover in a strong magnetic field applied in the Faraday geometry; see Fig. 2(c). However, the characteristic fields differ from each other: $B_{1/2}^V = 0.5$ mT (from RSA width) and $B_{1/2}^F = 3.9$ mT (from PR curve). The underlying mechanisms are the subject of further investigations.

V. DISCUSSION

We interpret the decrease of the PR amplitude for increasing modulation frequency, shown in Figs. 2(d) and 3(a), as a decrease of the electron spin polarization due to the spin inertia effect. The red lines in Fig. 3(a) are fits to the data according to Eq. (11). From these fits we obtain spin lifetimes of $T_S = 1.5$ and 1.0 μs for low and high pump density, respectively. The pump density dependence of T_S is described by Eq. (2). Keeping in mind that $\tau = n_0/G$, one sees that for vanishing pump rates G the term $1/\tau \to 0$ and $T_S \to \tau_S$. This provides a way to measure the spin relaxation time τ_S. Figure 3(b) shows the inverse spin lifetime $1/T_S$ in dependence on the pump density. From it we extrapolate $\tau_S = (1.6 \pm 0.1)$ μs at $T = 1.8$ K and $B_F = 5$ mT.

The evaluated spin relaxation time τ_S in dependence on the magnetic field is shown in Fig. 4(a) for the range of weak magnetic fields $B_F < 20$ mT. It is constant in this field range at $\tau_S = 1.6$ μs. Note in particular that it is also constant below 5 mT where the electron spin polarization decreases considerably due to the fluctuating nuclear magnetic field as can be seen from the black line which shows the corresponding PR signal at $f_m = 75$ kHz. Furthermore, the results presented in Figs. 4(a) and 4(c) suggest that the spin lifetime T_S and, correspondingly, the spin relaxation time τ_S do not depend on B_F in the whole range from zero up to 2.5 T. Note, that this is a rather unexpected result as commonly the carrier spin relaxation time is sensitive to the application of magnetic

fields. Figure 5 demonstrates another surprising observation, namely that the spin relaxation time does not depend on the temperature in the range from 1.8 to 45 K.

Let us discuss possible spin relaxation mechanisms that can be responsible for this behavior. For that we compare the characteristic times of the electron spin dynamics determined by the various techniques and discuss the spin relaxation mechanisms which can describe the measured properties of electron spins bound to fluorine donors in ZnSe. Comparing the results of the different techniques we find that $\tau_S \gg T_2^*$; i.e., the characteristic time determined from the Hanle curve T_2^* and the irreversible spin relaxation time τ_S determined from the spin inertia method strongly differ. This can be explained by the broadening of the Hanle curve due to the nuclear spin fluctuations: The strongly localized, donor-bound electrons in the fluorine-doped ZnSe epilayers interact with the nuclear hyperfine field of the same nuclei for a long time ($\tau_c \geqslant \hbar/(\mu_B g_e B_N)$). The resulting Larmor precession in the nuclear hyperfine field broadens the Hanle curve, so that the spin lifetime obtained from the Hanle measurement is limited by this reversible effect and is much shorter than the time for the irreversible spin relaxation τ_S determined from the spin inertia method.

Every mechanism of irreversible spin relaxation can be interpreted as the effect of fluctuating magnetic fields on the electron spin. Equation (4) is valid in the case of fastly varying magnetic field $\tau_c \ll \tau_S$, when dynamical averaging takes place. In a strong magnetic field the relaxation times of the longitudinal and transverse components T_1 and T_2 are different. The time T_1 describes the decay of the spin component along the magnetic field. This time can depend considerably on the magnetic field, since the spin-flip requires the transfer of the energy $\mu_B g_e B$ to the lattice. On the contrary, the time T_2 describes the decoherence time, which is not related to an energy transfer to the lattice. They become equal to each other $T_1 = T_2 = \tau_S$ in a weak magnetic field [14]. The spin relaxation time τ_S that we determine with the spin inertia method with the magnetic field applied in Faraday geometry is the T_1 time.

For sufficiently strong longitudinal magnetic fields one would expect a dependence of the spin relaxation time on the magnetic field. However, we do not observe any dependence of τ_S on the magnetic field from zero up to 2.5 T for the donor-bound electrons and only small variations within the accuracy of our method in the temperature range from 1.8 up to 45 K. This imposes severe restrictions on the fluctuating magnetic fields, which can be used to describe the spin relaxation process. Calculating the Zeeman splitting of the electron states at an external magnetic field of $B = 2.5$ T we can deduce that the fluctuations of the random magnetic field describing the underlying relaxation mechanism must have a wide frequency range $\mu_B g_e B/\hbar \approx (3 \text{ ps})^{-1}$. Thus, the correlation time of the corresponding fluctuating field must be shorter than 3 ps.

The following, almost instantaneous processes can be considered: (i) scattering between free and donor-bound electrons (the exchange interaction between the electrons is responsible for the electron spin flip), (ii) jumping of electrons between different donors (hyperfine and spin-orbit interaction), (iii) scattering of phonons by donor-bound electrons (spin-

orbit interaction), and (iv) charge fluctuations in the environment of the donors (spin-orbit interaction). All of them will be discussed in the following.

The process (i) is unlikely, because the localized states are excited resonantly and the donor ionization process should depend on the temperature in the range from 30 to 50 K, which does not reflect the experimental observations.

The process (ii) can be provided by two mechanisms: electron spin flip-flop transitions, which are induced by the scalar exchange interaction between electrons on neighboring donors, and electron jumps of donor-bound electrons to unoccupied donors. Calculations according to Ref. [27] for the parameters of the fluorine donor in ZnSe yield a jump time which is much longer than the estimated 3 ps. Thus, we discard option (ii) as a possible mechanism.

We also discard the process (iii), since we do not observe any temperature dependence of the spin relaxation time τ_S, which we would expect for a phonon-mediated process.

The only possible mechanism left is the process (iv), charge fluctuations in the environment of the donors, which, e.g., might occur during the 1.5 ps duration of the laser pulse illumination. We test this possibility by changing the pulsed pump beam to cw excitation. However, the determined spin relaxation time still does not depend on magnetic field or on temperature in the specified range. According to this check we can exclude a direct influence of the pulsed excitation on the spin relaxation. However, we cannot completely disregard any illumination-induced mechanism, as charge fluctuations can be produced also by cw laser excitation in combination with carrier recombination during tens of picoseconds [3]. Still, there is no clear evidence for this so that we suggest that there may be a different, new mechanism, which determines the spin relaxation time in this system with strong electron localization.

VI. CONCLUSIONS

We have suggested a method based on the spin inertia effect to measure the longitudinal spin relaxations time T_1 of carriers. It exploits optical orientation of the carrier spins and their polarization recovery in a magnetic field in the Faraday geometry, measured for different helicity modulation frequencies. The validity of this method is demonstrated for electrons bound to fluorine donors in ZnSe. An electron spin relaxation time of $T_1 = 1.6$ μs is measured in the temperature range 1.8–45 K. This time remains constant for magnetic fields varied from zero to 2.5 T. Measurements of the spin dephasing time $T_2^* = 33$ ns with the RSA technique, and a comparison of pulsed and continuous-wave excitation, allow us to conclude that the spin relaxation of the donor-bound electrons is caused by perturbations that cover a broad spectral range. The question about the origin of this perturbation has remained open so far and needs further investigations.

The obvious advantage of the suggested polarization recovery technique based on the spin inertia effect is that it is suitable for measuring the longitudinal spin relaxation time T_1 in the whole range of magnetic field starting from zero field. Contributions of different spin relaxation mechanisms may be distinguished by their different onsets in the modulation

frequency dependence. This distinction is possible when the generated carrier spin polarization is not fully destroyed by a faster relaxation mechanism. A requirement for the suggested technique is the finite optical orientation of carriers (at least of about a few percent that can be comfortably detected). The photoinduced carrier spin polarization can be detected by various methods, e.g., by Kerr or Faraday rotation or by the circular polarization degree of photoluminescence. The main limitation of the technique comes from the condition that the pump helicity modulation period shall be tuned to a time shorter than the spin lifetime T_S. Therefore, the technique can be well applied to measure long relaxation times, e.g., of resident carriers, but it is less suited for fast-decaying excitons, for example, whose typical recombination time is shorter than

a nanosecond, as it would require a modulation frequency exceeding 1 GHz.

[1] K. Sanaka, A. Pawlis, T. D. Ladd, D. J. Sleiter, K. Lischka, and Y. Yamamoto, Nano Lett. **12**, 4611 (2012).

[2] D. J. Sleiter, K. Sanaka, M. Kim, K. Lischka, A. Pawlis, and Y. Yamamoto, Nano Lett. **13**, 116 (2013).

[3] Y. M. Kim, D. Sleiter, K. Sanaka, D. Reuter, K. Lischka, Y. Yamamoto, and A. Pawlis, Curr. Appl. Phys. **14**, 1234 (2014).

[4] D. D. Awschalom, D. Loss, and N. Samarth (eds.), *Semiconductor Spintronics and Quantum Computation* (Springer-Verlag, Berlin, 2002).

[5] M. I. Dyakonov and V. I. Perel, in *Optical Orientation*, edited by F. Meier and B. P. Zakharchenya (North-Holland, Amsterdam, 1984), Chap. 2.

[6] W. Hanle, Z. Phys. **30**, 93 (1924).

[7] C. Cohen-Tannoudji and A. Kastler, in *Progress in Optics*, Vol. 5, edited by E. Wolf (North-Holland, Amsterdam, 1966).

[8] R. R. Parsons, Phys. Rev. Lett. **23**, 1152 (1969).

[9] W. Happer, Rev. Mod. Phys. **44**, 169 (1972).

[10] E. B. Aleksandrov, Sov. Phys. Usp. **15**, 436 (1973).

[11] D. Budker, W. Gawlik, D. F. Kimball, S. M. Rochester, V. V. Yashchuk, and A. Weis, Rev. Mod. Phys. **74**, 1153 (2002).

[12] R. I. Dzhioev, V. L. Korenev, I. A. Merkulov, B. P. Zakharchenya, D. Gammon, Al. L. Efros, and D. S. Katzer, Phys. Rev. Lett. **88**, 256801 (2002).

[13] I. A. Merkulov, Al. L. Efros, and M. Rosen, Phys. Rev. B **65**, 205309 (2002).

[14] A. Abragam, *The Principle of Nuclear Magnetism* (Oxford University Press, Oxford, 1961).

[15] J. S. Colton, D. Meyer, K. Clark, J. Cutler, T. Park, and P. White, J. Appl. Phys. **112**, 084307 (2012).

[16] I. A. Akimov, D. H. Feng, and F. Henneberger, Phys. Rev. Lett. **97**, 056602 (2006).

[17] I. A. Akimov, D. H. Feng, and F. Henneberger, in *Semiconductor Quantum Bits*, edited by F. Henneberger and O. Benson (Pan Stanford Publishing, Singapore, 2009), Chap. 4.

[18] F. Fras, B. Eble, P. Desfonds, F. Bernardot, C. Testelin, M. Chamarro, A. Miard, and A. Lemaitre, Phys. Rev. B **84**, 125431 (2011).

[19] A. Greilich, A. Pawlis, F. Liu, O. A. Yugov, D. R. Yakovlev, K. Lischka, Y. Yamamoto, and M. Bayer, Phys. Rev. B **85**, 121303(R) (2012).

[20] E. A. Zhukov, O. A. Yugov, I. A. Yugova, D. R. Yakovlev, G. Karczewski, T. Wojtowicz, J. Kossut, and M. Bayer, Phys. Rev. B **86**, 245314 (2012).

[21] J. M. Kikkawa and D. D. Awschalom, Phys. Rev. Lett. **80**, 4313 (1998).

[22] I. A. Yugova, M. M. Glazov, D. R. Yakovlev, A. A. Sokolova, and M. Bayer, Phys. Rev. B **85**, 125304 (2012).

[23] J. L. Merz, H. Kukimoto, K. Nassau, and J. W. Shiever, Phys. Rev. B **6**, 545 (1972).

[24] E. A. Zhukov, A. Greilich, D. R. Yakovlev, K. V. Kavokin, I. A. Yugova, O. A. Yugov, D. Suter, G. Karczewski, T. Wojtowicz, J. Kossut, V. V. Petrov, Y. K. Dolgikh, A. Pawlis, and M. Bayer, Phys. Rev. B **90**, 085311 (2014).

[25] G. V. Astakhov, M. M. Glazov, D. R. Yakovlev, E. A. Zhukov, W. Ossau, L. W. Molenkamp, and M. Bayer, Semicond. Sci. Technol. **23**, 114001 (2008).

[26] M. Y. Petrov, I. V. Ignatiev, S. V. Poltavtsev, A. Greilich, A. Bauschulte, D. R. Yakovlev, and M. Bayer, Phys. Rev. B **78**, 045315 (2008).

[27] K. V. Kavokin, Semicond. Sci. Technol. **23**, 114009 (2008).